Polypeptide Diblock Copolymers: Syntheses and Properties of Poly(*N*-isopropylacrylamide)-*b*-Polylysine

Cheng-Jyun Huang and Feng-Chih Chang*

Institute of Applied Chemistry, National Chiao Tung University, Hsinchu, Taiwan

Received June 1, 2008; Revised Manuscript Received July 7, 2008

ABSTRACT: A hydrolysis-resistant amide-linkage heterofunctional initiator was synthesized and used successfully for polymerization of well-defined rod−coil block copolymers poly(*N*-isopropylacrylamide)-*b*-poly(Z-L-lysine) (PNIPAm-*b*-PZLys) by combination of atom transfer radical polymerization (ATRP) and amine hydrochloride mediated ring-opening polymerization (ROP). The ATRP of NIPAm was carried out at 0 °C using CuBr/Me_6TREN complex in 2-propanol and resulted in narrow polydispersity and high monomer conversion. The amine hydrochlorides have replaced the primary amine in the PNIPAm macroinitiator resulting in a well-controlled ROP of N^{ε}-(carbobenzoxy)-L-lysine *N*-carboxyanhydride in DMF at 20 °C. These amphiphilic block copolymers are able to form universal micelle morphologies of spherical micelles, wormlike micelles, and vesicles by varying the polymer compositions and the helicogenic common solvents. From synchrotron SAXS, WAXS, and TEM results, the PNIPAm-*b*-PZLys microphase self-assembly morphology in solid state is a hierarchical lamellar-in-hexagonal structure. After the protective ε-benzyloxycarbonyl group is removed, the dual stimuli-responsive behaviors of the PNIPAm-*b*-PLys investigated by nuclear magnetic resonance spectroscopy in aqueous solution resulted in either coil-to-helix or coil−globule transition by changing the environmental condition of elevating the temperature or increasing the pH value.

Introduction

Self-assembly of block copolymers, driven by the incompatibility of constituents, into ordered structures in solution and solid state in the submicrometer range provides a route to hierarchical nanostructure materials with a variety of potential applications.[1] Biomimetic stimuli-responsive block copolymers capable of self-assembly in aqueous solution are particularly interesting as their promising potential in variety of applications such as in drug delivery,[2] in biotechnology,[3] and in the development of sensors.[4] These "smart" materials can reversibly change their physicochemical properties in response to variations in temperature,[5] pH,[6] or ionic strength.[7]

Block copolymers comprised of polypeptide segments have shown significant advantages in controlling functional and supramolecular structures of bioinspired self-assemblies in aqueous solution.[8] Peptide copolymers provide many advantages over conventional synthetic polymers due to their ability to hierarchically assemble into stable ordered conformations. With different amino acid substitutions, polypeptides can adopt well-defined stable secondary structures such as the α-helix, β-sheet, or coil depending on external environment.[9] Therefore, the hybrid copolymers (also named molecular "chimeras")[10] combining various conventional synthetics of specific functionalities with polypeptides have been intensively investigated.[11]

To be successful in these purposes, it is important that materials can self-assemble into precise and predictable structures. Since the late 1940s, the ring-opening polymerization (ROP) of α-amino acid *N*-carboxyanhydrides (NCAs) initiated by nucleophiles or bases have been the most common technique used for polypeptides preparation.[12] However, an attempt to prepare polypeptides always results in unmatched compositions with monomer feed ratios and significant homopolymer contaminants because of the nucleophilic/basic duality of the initiator. Elimination of these side reactions has been the major synthetic challenge for this polymerization system.[13] Several innovative approaches have been proposed for controlling NCA polymerization by different concepts. Deming reported replacing primary amine initiators with organonickel initiators which are able to give controllable polymerization of a wide range of NCA monomers from pure enantiomers to racemic mixtures.[14] Sequential addition of different NCA monomers enables preparation of block copolypeptides with defined sequence and composition. Recently, Deming et al. also described the first use of a macroinitiator bearing amido−amidate nickel cycle end groups to synthesize hybrid block copolymers.[15] Both Hadjichristidis and Schlaad groups reported the conventional primary amine-initiated polymerization of NCAs with distinct ideals. The former employed their high-vacuum technique to create and maintain conditions necessary for the living polymerization of NCAs.[16] Their approaches of controlling the reaction conditions resolved the existing problem for more than 50-year-old challenge presented by the NCA/nucleophile system. The latter group's strategy is to avoid the "activated monomer" pathway by simply adding protons, provided that fast reprotonation of the eventually formed NCA anions is faster than the nucleophilic attack of another NCA molecule, thus eliminating the side reaction.[17] This approach has been applied by other groups to synthesize well-defined hybrid copolymers.[18]

In order to incorporate desired functional segments into polypeptides-based copolymers, additional polymerization techniques are required. Controlled/living radical polymerization (CRP), developed in the past decade,[19] enables the facile synthesis of polymers with controlled molecular weight, low polydispersity, and well-defined architecture. Additionally, desired functionalities can be incorporated into either end group or distributed along polymer backbone. Since ROP and CRP are distinct mechanisms, a dual heterofunctional initiator[20] to combine these two routes is important to design and synthesize various hybrid block copolymers.

Few research activities have been focused on dual stimuli-responsive hybrid block copolymers consisting of pH-sensitive polypeptides and thermo-sensitive segment.[21] Poly(*N*-isopropylacrylamide) (PNIPAm), the most widely studied thermo-responsive polymer, exhibits coil-to-globule transition above the lower critical solution temperature (LCST) at 32 °C in aqueous solution. Below this critical temperature, it is in a hydrophilic

* Corresponding author. E-mail: changfc@mail.nctu.edu.tw.

10.1021/ma801221m CCC: $40.75
Published on Web 09/06/2008

Scheme 1. Synthesis of Phthalimidoethyl 2-Bromo-2-methylpropionamide Hetero-Functional Initiator (2)

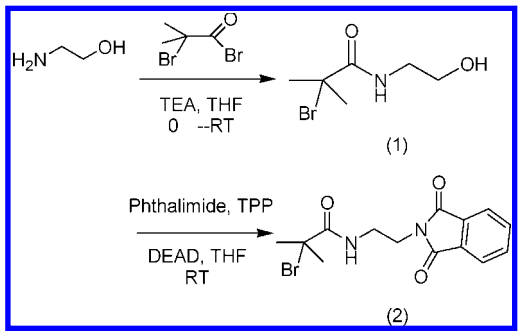

state, and above this temperature it is in a hydrophobic state.[22] All the major CRP techniques, atom transfer radical polymerization (ATRP),[23] nitroxide-mediated polymerization (NMP),[24] and reversible addition−fragmentation chain transfer polymerization (RAFT),[25] have been successfully used to prepare poly(*N*-isopropylacrylamide) with low-to-moderate chain length and narrow molecular weight distribution.

In this paper, we report the synthesis of a new amide-linkage phthalimidoethyl 2-bromo-2-methylpropionamide heterofunctional initiator which allows both polymerizations to be conducted consecutively by ATRP then the amine hydrochloride mediated ROP of N^{ε}-(carbobenzoxy)-L-lysine *N*-carboxyanhydride (Z-Lys-NCA) or γ-benzyl L-glutmate *N*-carboxyanhydride (BLG-NCA) to synthesize well-defined poly(*N*-isopropylacrylamide)-*b*-polypeptide hybrid block copolymers. An investigation of these rod−coil hybrid block copolymers' self-assembly and solution behaviors is preliminarily presented including the dual stimuli-responsive of pH and thermo-sensitive behaviors in aqueous solution after removing the protective Cbz-group, the amphiphilic block copolymer self-assembly in different helicogenic common solvent, and the hierarchical nanostructure in solid state.

Experimental Methods

Materials. All reagents and solvents were purchased from commercial suppliers and used as received unless otherwise noted, including L-glutamic acid 5-benzyl ester (Fluka, >99%), N^{ε}-(carbobenzoxy)-L-lysine (ACROS, 98%), triphosgene (TCI, >98%), ethanolamine (Tedia, 99%), bromoisobutyryl bromide (ACROS, 98%), diethyl azodicarboxylate solution 40% in toluene (Fluka), triphenylphosphine (Lancaster, 99%), phthalimide (ACROS, 98%), hydrazine monohydrate (Sigma-Aldrich, 98%), 2-propanol (Tedia, 99.5%), uranyl acetate dihydrate (Fluka, 98%), hydrogen bromide 33 wt % in acetic acid (ACROS), and trifluoroacetic acid (ACROS, 99%). The monomer *N*-isopropylacrylamide (NIPAm, 99%, TCI) was recrystallized in hexane/toluene, and dried under vacuum before use. Ethyl acetate (Tedia, 99.8%) and *N*,*N*-dimethylformamide (DMF; Tedia, 99.8%) were dried over CaH_2 (ACROS, 93%) and distilled under reduced pressure. Tetrahydrofuran (Tedia, 99.8%) was distilled over Na/benzophenone. Deioned (DI) water used in all reactions, solution preparations, and polymer isolations was purified to a resistance of 18 MΩ (Milli-Q Reagent Water System, Millipore Corp.). N^{ε}-(carbobenzoxy)-L-lysine *N*-carboxyanhydride (Z-L-lysine NCA) and γ-benzyl L-glutmate *N*-carboxyanhydride (BLG NCA) were synthesized according to the method described by Poché et al. (Fuchs−Farthing method).[26] Hexamethylated tris(2-(dimethylamino)ethyl)amine (Me_6TREN) was synthesized according to method of Ciampolini.[27]

Synthesis of 2-Bromo-*N*-(2-hydroxyethyl)-2-methylpropionamide (BrPA) (1) (Scheme 1. Ethanolamine (5.31 g, 86.9 mmol, 1.0 equiv) and TEA (8.8 g, 173.8 mmol, 2.0 equiv) dissolved in THF (400 mL) were fed into a 500 mL two-necked round-bottomed flask fitted with a Ar inlet and a rubber septum and were cooled in an ice bath. The α-bromoisobutyryl bromide (20 g, 86.9 mmol, 1.0 equiv) was added into the mixture dropwise. White precipitate of triethylammonium bromide was observed and the reaction was allowed to stir at room temperature overnight. After the precipitate was filtered off, THF was removed by rotary evaporation. The residue was purified with column chromatography (silica gel, hexane/ethyl acetate v/v: 1/1) yield product 1 (11.33 g, 62%) as a viscous oil. ^{1}H NMR ($CDCl_3$, δ, ppm) 7.13)(br, 1H, −N*H*−), 3.72 (m, 2H, HO−CH_2−), 3.42 (m, 2H, HO−CH_2−CH_2−), 2.32 (br, 1H, *H*O−CH_2−), 1.93 (s, 6H, Br(CH_3)$_2$−C−). ^{13}C NMR ($CDCl_3$, δ, ppm): 173.12 (−NH−*C*(O)−C−), 62.51 (Br(CH_3)$_2$−*C*−C(O)−), 61.77 (HO−*C*H_2−CH_2−), 42.97 (HO−CH_2−*C*H_2−), 32.48 (Br(*C*H_3)$_2$−C−).

Synthesis of Phthalimidoethyl 2-Bromo-2-methylpropionamide (PIBrPA) (2) (Scheme 1). To a THF solution (250 mL) of a mixture of product (**1**) (9 g, 42.8 mmol, 1.0 equiv), triphenylphosphine (14.6 g, 55.6 mmol, 1.3 equiv), phthalimide (6.3 g, 42.8 mmol, 1.0 equiv) was added dropwise 40% toluene solution of diethylazodicarboxylic acid (DEAD; 24.3 g, 55.6 mmol, 1.3 equiv), and the resulting mixture was stirred under argon at room temperature for 12 h. The reaction mixture was then evaporated to dryness, and the residue was purified with column chromatography (silica gel, hexane/ethyl acetate v/v: 4/1) and recrystallized with THF/hexane to yield product (2) (6.5 g, 45%) as a white needle-like crystals. ^{1}H NMR ($CDCl_3$, δ, ppm): 7.86 (m, 2H, phthalyl aromatic), 7.70 (m, 2H, phthalyl aromatic), 7.09 (br, 1H, −N*H*−), 3.87 (m, 2H, −CH_2−CH$_2$−NH−), 3.54 (m, 2H, −CH_2−CH_2−NH−), 1.85 (s, 6H, Br(CH_3)$_2$−C−). ^{13}C NMR ($CDCl_3$, δ, ppm): 172.44 (−NH−*C*(O)−C−), 168.43 (−C−*C*(O)−N−), 134.12, 131.86, 123.38 (aryl-*C*), 62.13 (Br(CH_3)$_2$−*C*−C(O)−), 39.82 (−CH_2−CH$_2$−NH−),37.16(−CH$_2$−*C*H$_2$−NH−),32.23(Br(*C*H$_3$)$_2$−C−).

Preparation of Phthalimide End-Capped Poly(*N*-isopropylacrylamide) (3) by ATRP (Scheme 2). A typical polymerization procedure of NIPAm at monomer/initiator ratio of 250 was as carried out follows. NIPAm (4.00 g, 35.40 mmol), initiator (0.048 g, 0.14 mmol), and 2-propanol (7.65 mL) were combined and deoxygenated by performing freeze−pump−thaw cycles. Upon equilibration at 20 °C after the third cycle, the flask was immersed into a water or ice bath. To allow the buildup of the complex between the metal and ligand, an oxygen-free solution of 2-propanol (2.55 mL) containing CuBr or CuCl (20.5 mg or 14.16 mg, 0.1416 mmol) and Me_6TREN (32.7 mg, 38.85 μL) was prepared separately. This solution was then added to the monomer and initiator mixture via an argon-washed syringe to start polymerization. The reaction mixture was exposure to air to stop polymerization, then evaporated to dryness, and the residue was dissolved in 150 mL of THF, and the copper catalyst was removed by passing through a neutral alumina column. The solution was concentrated and precipitated in *n*-hexane to yield PNIPAm as white powder. To obtain the actual M_n calculated from the ratio of the integral of the phthalimide and methine protons peak by ^{1}H NMR, the phthalimide end-capped PNIPAm was further purify by dialysis against DI water to exclusively eliminate residual monomer and noninitiated initiator. ^{1}H NMR (500 MHz, $CDCl_3$): δ 1.12 (br, CH(CH_3)$_2$) 1.33−2.24 (br, aliphatic *H*) 3.98 (br, C*H*(CH_3)$_2$), 6.63 (br, N*H*), 7.71 (br, phthalyl aromatic), 7.81 (br, phthalyl aromatic).

Hydrazinolysis of Phthalimide End-Capped PNIPAm to Primary Amine (4a) and Amine Hydrochloride-Functionalized PNIPAm (4b) (Scheme 2). Phthalimide end-capped PNIPAm (5 g) and 5-folds excess hydrazine monohydrate were dissolved in ethanol (25 mL) and the mixture was stirred at room temperature under argon for 12 h. (upon the addition of the hydrazine, the solution became yellowish due to the formation of phthalyl hydrazide.) The mixture was placed in a dialysis bag (MWCO = 3500 Da) and dialyzed against DI water for 48 h. The DI water was changed every hour for the first 5 h. Finally the water solution was freeze-dried. Isolated yield: 2.3 g (46%). To convert primary amine into amine hydrochloride, excess amount of 1 M HCl was added into the mixture solution and stirred for 2 h to convert primary amine into amine hydrochloride. The mixture was dialyzed and

Scheme 2. Synthesis of Poly(*N*-isopropylacrylamide)-*b*-polypeptides

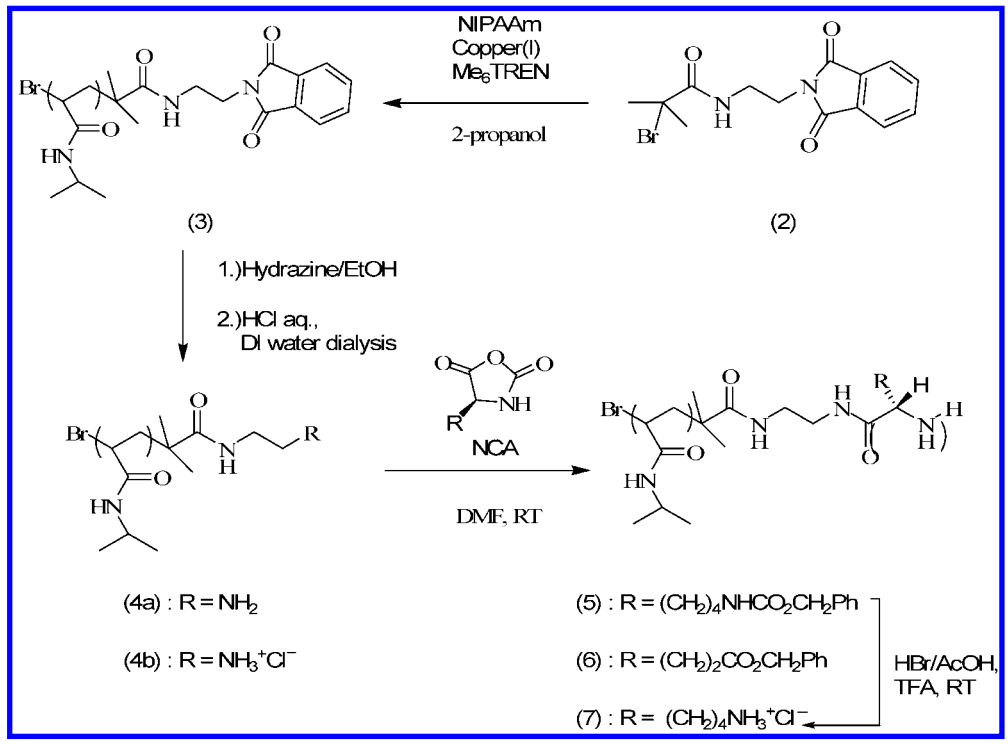

Table 1. Experimental Conditions and Properties of PNIPAm Prepared by ATRP: Effect of Catalyst and Temperature

entry	monomer/initiator	catalyst	temp (°C)	time (min)	conv[b]	M_n (g/mol) NMR[c]	M_n (g/mol) GPC	M_w/M_n
1[a]	250/1	CuBr	20	70	56.19	15 874	17 747	1.31
2[a]	250/1	CuCl	20	250	70.25	19 846	19 379	1.32
3[a]	250/1	CuBr	0	720	63.88	18 046	18 444	1.12

[a] Ratio of reactants: $[NIPAAm]_0/[PIBrPA]_0/[Cu(I)]_0/[Me_6TREN]_0$ = 250/1/1/1; $[NIPAAm]_0$ = 3.473 M, in 2-propanol (2.0 weight equiv vs mono-mer). [b] Monomer conversion was determined from the ^1H NMR integration ratio of the monomer double bond at 5.5 ppm to polymer peak at 3.8 ppm in DMSO-d_6. [c] $M_{n,NMR}$ = ($[NIPAAm]_0/[PIBrPA]_0$) × conversion × $M_{monomer}$.

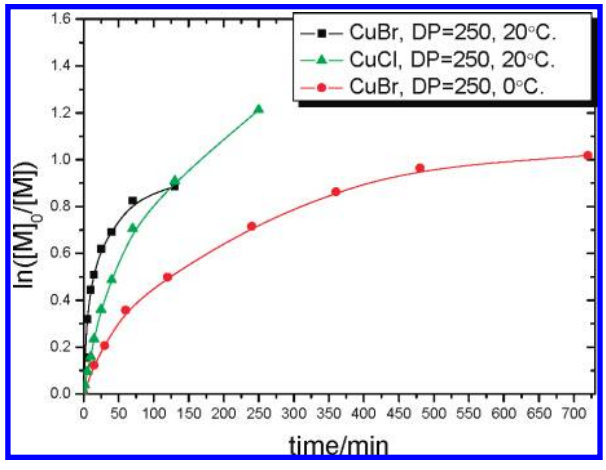

Figure 1. Kinetic plots for the polymerization of NIPAAm at different temperatures and catalyzed by different copper catalysts.

lyophilized. The amine hydrochloride-functionalized PNIPAm isolated yield: 2.6 g (52%). ^1H NMR (500 MHz, D_2O): δ 1.05 (br, $CH(CH_3)_2$), 1.50 (br, $-CHCH_2-$), 1.92 (br, $-CHCH_2-$), 3.02 (br, $-CH_2-CH_2-NH_3^+Cl-$), 3.39 (br, $-CH_2-CH_2-NH_3^+Cl-$), 3.81 (br, $CH(CH_3)_2$).

General Procedure for Synthesis of Poly(*N*-Isopropylacrylamide-*b*-peptide) Block Copolymer (5, 6) by ROP Polymerization (Scheme 2). Typically, the functionalized PNIPAm macroinitiator and *N*-carboxyanhydride monomer were dried at room temperature in separated dried flask under high vacuum for 1 h. Then, two separate DMF solutions were prepared and subsequently combined via transfer needle under argon to give ~9 wt % solution. The mixture was stirred at room temperature for several days under inert argon atmosphere. After polymerization, the solvent was concentrated to a minimum amount under high vacuum. The concentrated DMF solution was precipitated in ether and subsequently dried under vacuum.

Deprotection of the ε-Benzyloxycarbonyl (Cbz Group) Side Chains in PNIPAm-*b*-PZLys (7) (Scheme 2). A round-bottom flask was charged with a solution of the appropriate PNIPAm-*b*-PZLys in trifluoroacetic acid (100 mg/ 3 mL). Then, a 4-fold molar excess of a 33 wt % solution of HBr in acetic acid was added, and the reaction mixture was stirred for 1 h at room temperature. Finally, the reaction mixture was precipitated in ether and repeatedly

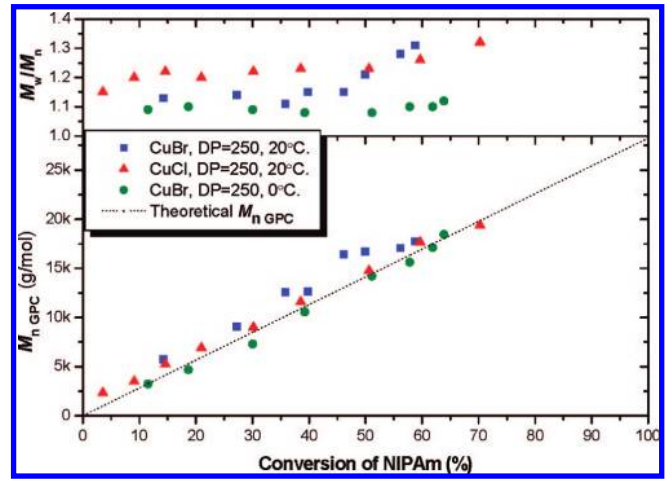

Figure 2. Molecular weights and polydispersities of PNIPAm as degree of conversion. Experimental conditions are given in Table 1.

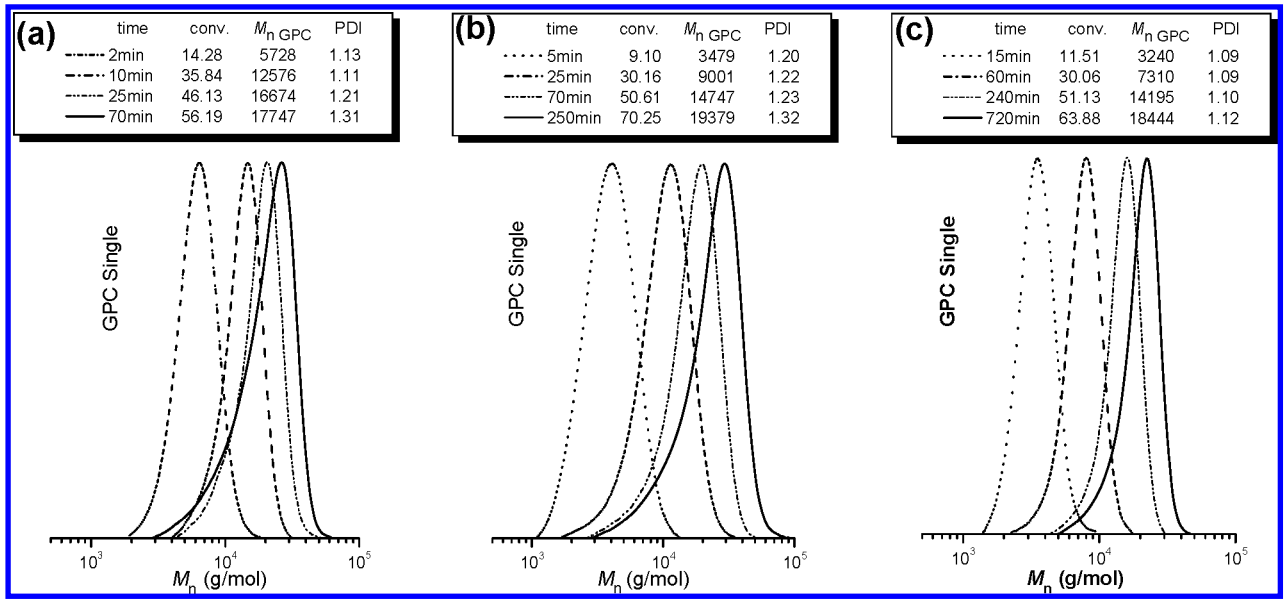

Figure 3. Evolution of the molecular weight GPC traces under different polymerization conditions: (a) CuBr/20 °C, (b) CuCl/ 20 °C, and (c) CuBr/0 °C.

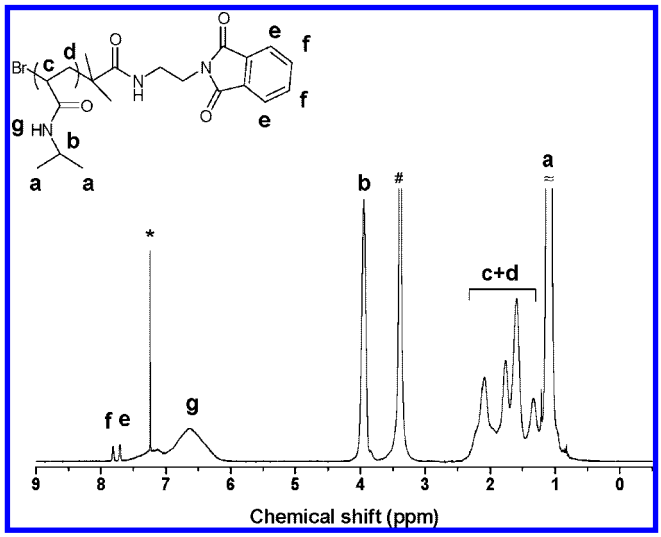

Figure 4. ^{1}H NMR spectrum of phthalimide end-capped poly(*N*-isopropylacrylamide) in $CDCl_3$ (*, $CDCl_3$; #, water).

dialyzed against water until the conductivity remains constant. The product was isolated via lyophilization.

Preparation Samples of Block Copolymer Micelles Assembled in Water. Dried solid block copolymer powder was dissolved in DMF or THF (1.0 mL) to give a 0.1% (w/v) solution. A stir bar was added followed by dropwise addition of DI water (0.1 mL) under constant stirring. The solution was allowed to stir for 48 h before exhaustive dialysis (Spectra/Por CE (cellulose ester) dialysis membranes, MWCO: 2000) against DI water for another 48 h to remove DMF or THF.

Preparation of Polymer Film. Polymer film was prepared by solvent casting 10% polymer solutions in DMF as a nonselective solvent. Liquid samples were placed on Teflon-coated aluminum foil (BYTAC) and were slowly dried within 5 days at 70 °C. The sample was scratched off the foil and isolated as transparent thin film.

Characterizations. ^{1}H NMR and ^{13}C NMR measurements were carried out at room temperature on a Varian Unity Inova spectrometer operating at 500 MHz using $CDCl_3$, DMSO-d_6, or D_2O as solvents. Monomer conversion was determined from the ^{1}H NMR integration ratio of the monomer double bond at 5.5 ppm to polymer peak at 3.8 ppm in DMSO-d_6. The molecular weight and molecular weight distribution were determined by gel permeation chromatography (GPC) using a Hitachi Pump L-7100—equipped with a RI 2000 refractive index detector, and three Ultrastyragel columns (100, 500, and 10^3 Å) connected in series in order of increasing pore size—using DMF as an eluent at a flow rate of 0.6 mL/min. The molecular weight calibration curve was obtained using polystyrene standards. Fourier transform infrared (FT-IR) spectra of solid samples were recorded at room temperature with a Nicolet AVATAR 320 FT-IR spectrometer. Transmission electron microscopy (TEM) images were obtained by using a JEOL JEM-2000EXII instrument operated at 120 kV. The sample was ultramicrotomed at room temperature using a diamond knife from Leica Ultracut UCT Microtome to give 70 nm thick sections and then transferred onto carbon-coated copper grids. For a selective staining of poly(Z-L-lysine), the specimens were exposed to the vapor of a freshly prepared aqueous RuO_4 solution. In micelles solution, one drop of each respective sample was placed on a 200 mesh Formvar-coated copper grid and allowed to remain on the grid for 120 s. Filter paper was then used to remove the residual sample and liquid. One drop of 2% (w/v) uranyl acetate (negative stain) was then placed on the grid, allowed to stain for 60 s, and subsequently removed by wicking away excess liquid with filter paper. The resulting samples were imaged by TEM. Wide-angle X-ray scattering (WAXS) spectrum was recorded on film sample using a Rigaku D/max-2500 type X-ray diffraction instrument. The radiation source used was Ni-filtered, Cu Kα radiation (λ = 1.54 Å). The sample was mounted on a circular holder, the scanning rate was 0.6°/min from 2θ = 1° to 80°. Data were collected and plotted as intensity versus scattering vector, q, where $q = (4\pi)\sin(\theta)$ and θ is the Bragg angle (or 1/2 the scattering angle). Small-angle X-ray scattering (SAXS) measurement was conducted on a dedicated setup at the end station of the BL17B3 beamline of the National Synchrotron Radiation Research Center (NSRRC), Taiwan. We used an X-ray beam of 0.5 mm diameter and a wavelength (λ) of 1.24 Å for the SAXS measurements.

Results and Discussion

Synthesis of Amide Linkage Heterofunctional ATRP Initiator. Since ester groups are good activating groups, α-haloester-based compounds are commonly used as ATRP initiators. In order to combine mechanistically incompatible initiation groups into ATRP initiator compound, usage of the robust amide linkage of α-haloamide-based initiator[28] is an alternative method to build up various architecture block

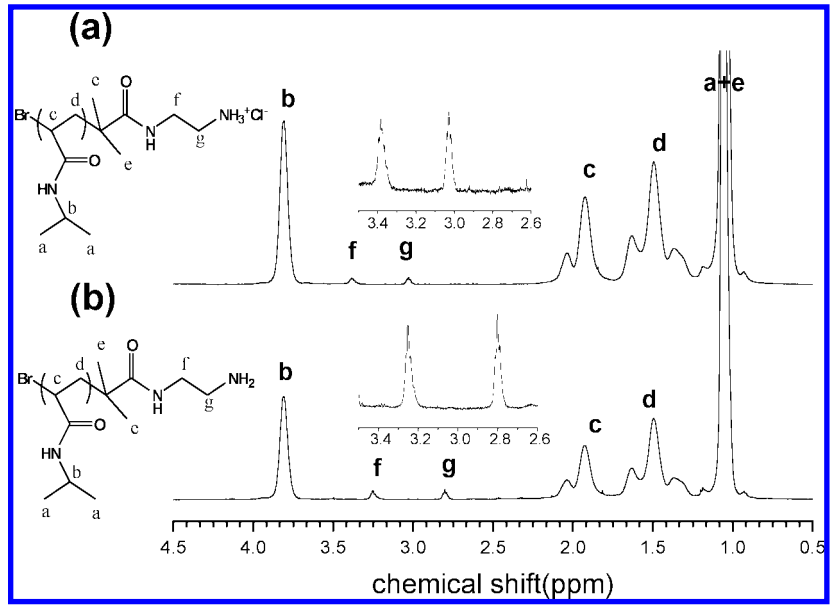

Figure 5. ^{1}H NMR spectra of (a) amine hydrochloride-functionalized PNIPAm macroinitiator and (b) amine-functionalized PNIPAm in D_2O at 25 °C; inset shows the amide methylene protons (f) and amine or amine hydrochloride methylene protons (g).

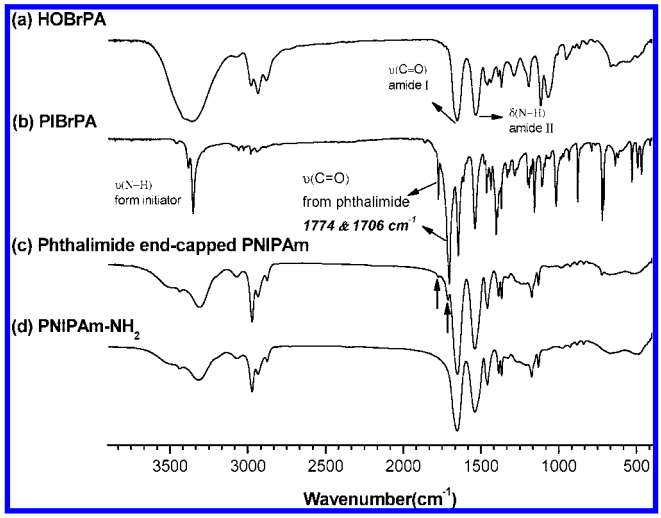

Figure 6. FT-IR spectra of (a) HOBrPA, (b) PIBrPA, (c) phthalimide end-capped PNIPAm, and (d) PNIPAm-NH_2.

copolymers. There have been several examples of using 2-bromo-2-methylpropionamide-based ATRP initiators to prepare various homopolymers and block copolymers.[29] In this study, α-bromo amide-based initiator was synthesized by amidation of the amino group of ethanolamine with α-bromoisobutyryl bromide and then the hydroxyl group was substituted by Mitsunobu reaction into phthalimide group which can be converted into amino group (Scheme 1). Accordingly, a new heterofunctional initiator was afforded for consecutive polymerization of *N*-isopropylacrylamide by ATRP and then ROP of amino acids NCA (Scheme 2).

Preparation of Phthalimide End-Capped Poly(*N*-isopropylacrylamide). Stöver and co-workers recently showed that ATRP of NIPAm in different alcohols, especially in 2-propanol, that alleviate catalyst inactivation by hydrogen bonding between amide groups and branched alcohols, led to narrow-disperse PNIPAm with high conversion and good molecular weight control.[23] Me_6TREN, a branched tetradentate ligand, forms one of the most active catalyst complex among all the ligands has been investigated, particular success in ATRP of acrylamides with good control over polymerization in room temperature.[30] In this study, the polymerization of NIPAm was investigated under a range of reaction conditions to investigate the catalysts and reaction temperature effect on ATRP. All reactions were conducted at the ratio of NIPAm/2-propanol = 1/2 (w/w) with Me_6TREN as ligand. When the Cu(I)Br was used to form the catalyst complex, the reaction was conducted at 20 °C for 70 min and yielded PNIPAm in 56.19% conversion with M_n = 17 747 g mol^{-1} and polydispersity (PDI) = 1.31. When the reaction was carried out with Cu(I)Cl at 20 °C, a halide exchange catalyst system,[31] polymerization for 250 min resulted in higher conversion of 70.25% with M_n = 19 846 g mol^{-1} (PDI = 1.32). At lower polymerization temperature at 0 °C, product with significant narrow molecular weigh distribution was achieved (PDI = 1.12) over 720 min with conversion of 63.88% and M_n = 18 444 g mol^{-1}. These polymerization data are summarized in Table 1. The reaction catalyzed by Cu(I)Br at 20 °C gives the fastest polymerization rate, and the kinetic plot is nonlinear (Figure 1, squares). This highly active Cu(I)Br/Me_6TREN has a large equilibrium constant in the ATRP and can rapidly initiate the initiators to generate high radical concentration at early stages of polymerization. Irreversible radical combination occurs continuously, and initiators are consumed until a sufficient number of the Cu(II)Br_2 deactivators are established to the activation/deactivation equilibrium. As a result, high persistent radical[32] concentration of Cu(I)Br_2 decreases the polymerization rate and increases the product PDI because active catalysts are insufficient for fast exchange between active and dormant chain ends. In addition, portion of the initiators produces low molecular weight polymer chains at the early stage of polymerization during the irreversible radicals combination, leading to lower initiation efficiency and higher PNIPAm molecular weight than theoretical values (Figure 2, squares). A small number of dead chains in Figure 3a suggests low initiation efficiency. In order to alleviate the fast polymerization rate, the halide exchange (R-Br/Cu(I)Cl) catalyst system was performed. Slower polymerization rate and a nonlinear kinetic plot were observed in this system (Figure 1, triangles). This is because stable terminal C−Cl bonds are formed from halide exchange during the propagation step. Therefore, the polymerization via R-Br/Cu(I)Cl system can achieve higher monomer conversion but gives a broad polydispersity similar to the R-Br/CuBr system (Figure 2, triangles).

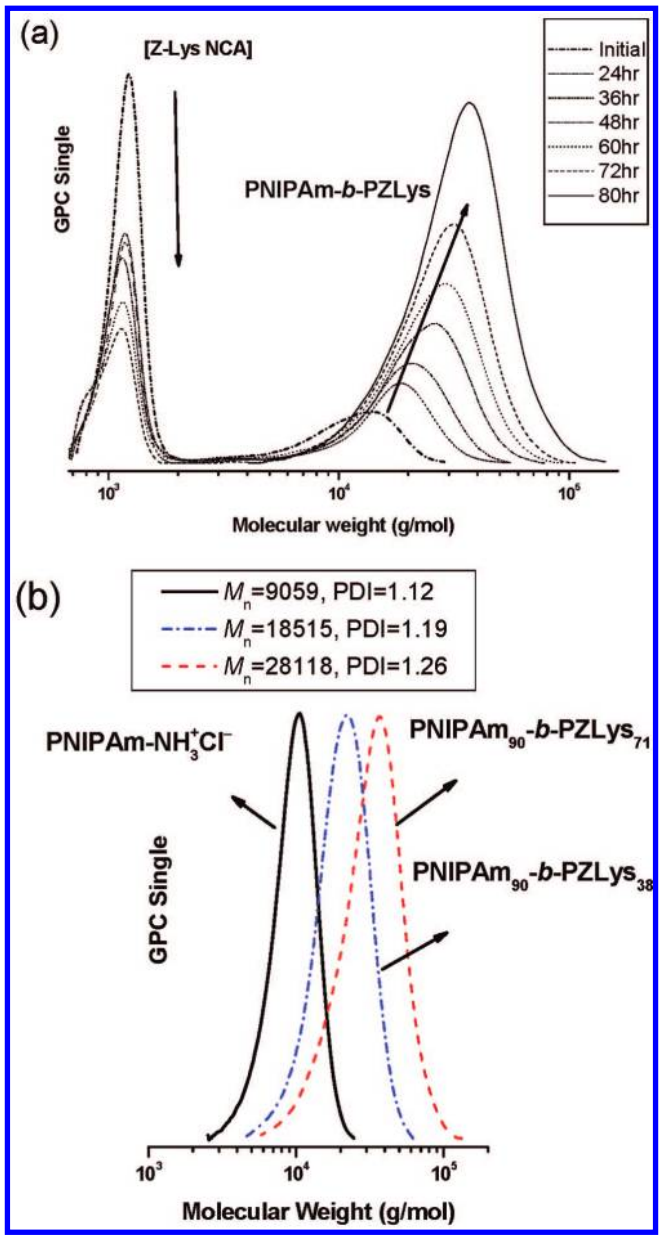

Figure 7. (a) GPC traces of monomer Z-Lys-NCA and PNIPAm$_{90}$-*b*-PZLys$_{90}$ (expt 2), (b) GPC signals of PNIPAm$_{90}$-*b*-PZLys$_{38}$, PNIPAm$_{90}$-*b*-PZLys$_{71}$, and PNIPAm-$NH_3^+Cl^-$ macroinitiator.

The polydispersity of polymers prepared by ATRP, reflecting the polymerization control, depends on the efficiency of deactivation according to[33]

$$\mathrm{PDI} = 1 + \left(\frac{k_p[\mathrm{RX}]_0}{k_{deact}[\mathrm{Cu^{II}X}]}\right)\left(\frac{2}{p} - 1\right) \quad (1)$$

where k_p is the propagation rate constant, k_{deact} is the deactivation rate constant, p is the monomer conversion, $[RX]_0$ is the initiator concentration, and $[Cu^{II}X]$ is the deactivator concentration. In general, the values of $k_{deact}[Cu^{II}X]$ are higher for X = Br than for X = Cl. Therefore, lower polydispersity is expected in systems in which alkyl bromide initiator and copper bromide-based catalysts are used.[32] Nevertheless, R-Br/Cu(I)Br system in this study produced molecular weights that deviated from theoretical values because of the high polymerization rate. Moreover, an improving R-Br/Cu(I)Cl system gives controllable living polymerization in contrast to the R-Br/Cu(I)Br system but the initial PDI has already increased to 1.20 for 5 min (Figure 3b). This can be attributed to the relatively slower rate of initiation reaction in the R-Br/Cu(I)Cl system compared with the R-Br/Cu(I)Br system, and thus deactivators are not enough to implement fast deactivation of active species to dormant polymer chains. In order to utilize the highly active Cu(I)Br/Me_6TREN possessing high efficiency in deactivation for narrow molecular weights distribution, polymerization of NIPAm with Cu(I)Br/Me_6TREN was also conducted at 0 °C. The kinetic plot (Figure 1, circles) shows that the polymerization rate is significantly reduced relative to the halide exchange system. The slow polymerization rate can be attributed to lower reaction temperature; however, a narrower molecular weight distribution is achieved (Figure 3c). The reaction reactivity at 0 °C still has high enough equilibrium constant to maintain the reactivity of Cu(I)Br/Me_6TREN, and the $Cu(I)Br_2$ deactivators provide effective deactivation rate to lower polydispersity according to eq 1. Although the kinetic plot is not linear, especially in the late stages of polymerization, the polydispersity remains narrow and the molecular weight linearly increases with conversion, indicating negligible loss of terminal alkyl halides. From the linearity of the $M_{n,GPC}$ versus conversion plot and low polydispersity, controllable polymerization of NIPAm can be achieved by ATRP using CuBr/Me_6TREN in 2-propanol at 0 °C.

The phthalimide end-capped PNIPAm was analyzed by ^{1}H NMR spectroscopy. The characteristic α-end phthalimide signals (e, f) derived from the initiator and other signals specific for polymer main chain protons are depicted in Figure 4. In addition, the M_n of the polymer was also determined from the PNIPAm methine protons ($-CH(CH_3)_3$)/phthalimide protons intensity ratios and the obtained values agree well with that determined by GPC. These results indicate that the heterofunctional initiator gives the end-functionalized PNIPAm by ATRP.

Hydrazinolysis of Phthalimide End-Capped PNIPAm. Primary amine and amine hydrochloride-functionalized PNIPAm were employed as macroinitiators for the anionic ring-opening polymerization of NCA to synthesize the diblock copolymers of PNIPAm-*b*-PZLys and PNIPAm-*b*-PBLG. The GPC profiles show that these two macroinitiators, PNIPAm-NH_2 and PNIPAm-$NH_3^+Cl^-$, dialyzed at different temperatures against DI water after hydrazinolysis (see Supporting Information for GPC traces, Figure S1). By comparing the molecular weight distribution of these two dialysis conditions, the coupling reaction in the presence of doubled molecular weight polymer arose during dialysis at ambient temperature 20 °C. The coupling reaction could be due to the nucleophilic substitution between the α-amine group and the terminal bromo group of PNIPAm.[34] We found that the nucleophilic substitution can be inhibited by dialyzing against cold water at 5 °C with negligible trace of coupling polymers in GPC analysis. For the phthalimide initiators utilized in previous studies, isomerization to 2-hydroxyethylamides on deprotection is a significant problem. This was pointed out first by Wooley[35] and then subsequently mentioned by Davis and co-workers.[36] However, according to the ^{1}H NMR spectra of these two α-functional macroinitiators shown in Figure 5, these two samples exhibit the characteristic α-end functional signals derived from the initiator after hydrazinolysis, including the amide methylene protons (f) and amine or amine hydrochloride methylene protons (g).

IR spectra for heterofunctional initiator, phthalimide end-capped PNIPAm, and PNIPAm-NH_2 are shown in Figure 6. The C═O characteristic peaks for the phthalimide group of initiator is at 1774 and 1706 cm^{-1} while peaks at 1644 and 1538 cm^{-1} are attributed to amide I and amide I bands. The spectrum of the phthalimide end-capped PNIPAm sample shows two phthalimide characteristic peaks, confirming that the ATRP is initiated by this initiator to form PNIPAm polymer. After hydrazinolysis of the phthalimide end-capped PNIPAm, the PNIPAm-NH_2 remains intact and only the phthalimide charac-

Table 2. Results of Synthesis Diblock Copolymers PNIPA-*b*-PZLys and PNIPAm-*b*-PBLG

PNIPAm-*b*-PZLys[a]

	macroinitiator [MI]							
expt	DP[b]	M_w/M_n	[Z-L-Lys NCA]$_0$/[MI]$_0$	time (h)	yield (%)	M_n (g/mol)	unit ratio *m*:*n*	M_w/M_n
1	90	1.12	45	80	80	18 515	90:38	1.19
2	90	1.12	90	35	75	28 118	90:71	1.26

PNIPAm-*b*-PBLG[a]

	macroinitiator [MI]							
expt	DP[b]	M_w/M_n	[BLG NCA]$_0$/[MI]$_0$	time (h)	yield (%)	M_n (g/mol)	unit ratio *m*:*n*	M_w/M_n
3	90	1.12	45	20	78	9327	90:37	1.39
4	90	1.12	90	45	58	13 025	90:55	1.43

[a] Polymerization at 20° in DMF (~9 wt %). [b] Calculated from the ratio of the integral of the amide methylene and methine protons peak by ^{1}H NMR.

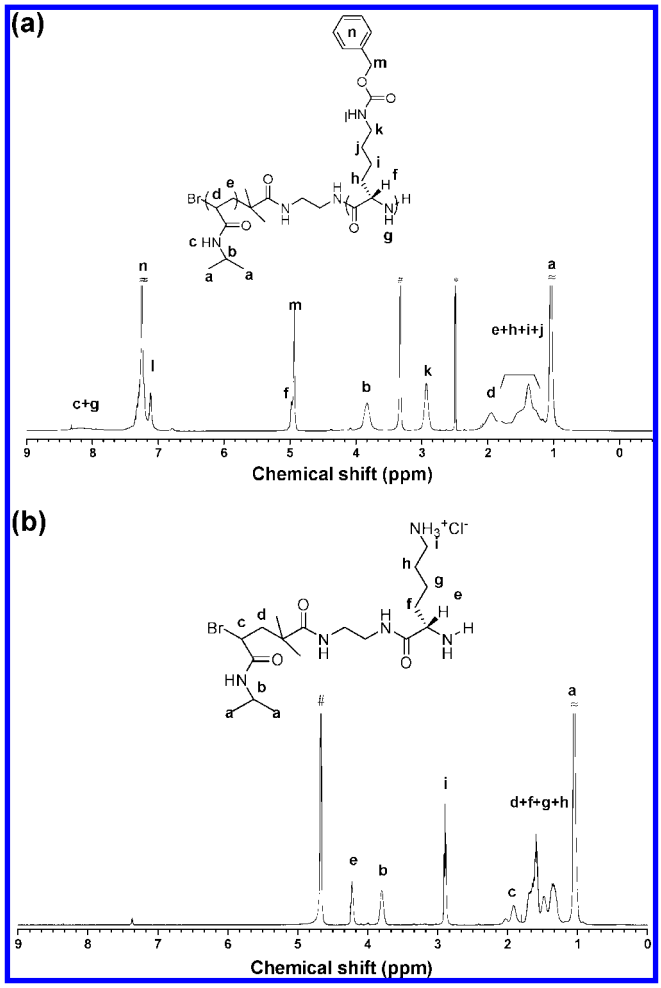

Figure 8. ^{1}H NMR spectra of (a) PNIPAm$_{90}$-*b*-PZLys$_{71}$ in dimethyl-d_6 sulfoxide at 25 °C and (b) PNIPAm$_{90}$-*b*-PLys$_{72}$ in D_2O at 25 °C (*, dimethyl sulfoxide; #, water).

teristic peaks are disappeared. In addition to NMR results, IR spectra further confirm our successful synthesis of the amine-functionalized PNIPAm macroinitiator.

Synthesis of Diblock Copolymer. By confirming the existence α-terminal functional groups by ^{1}H NMR, anionic ring-opening polymerization of NCA was performed by these two macroinitiators, GPC signals of PNIPAm-*b*-polypeptides via primary amine-functionalized PNIPAm (PNIPAm-NH_2, DP =125, M_n = 15 411 g mol^{-1}) are shown in Figure S2 (see Supporting Information for GPC analyses). These reactions can be completed within 24 h but are uncontrollable due to the inevitable activated monomer polymerization mechanism rather than normal amine mechanism. To eliminate the side reaction initiated by the nucleophilic/basic duality of primary amine, the primary amine-functionalized PNIPAm was replaced with amine hydrochloride-functionalized PNIPAm to prevent the activated monomer mechanism. The kinetic study of amine hydrochloride mediated ROP ([ZLys-NCA]$_0$/[MI]$_0$ = 90) is shown in Figure 7a by monitoring the GPC traces of monomer and molecular weight evolution of copolymers. Indeed, it clearly shows that the monomer signal intensity decreases and copolymer molecular weight increases simultaneously. The polymerization rate slows down (completed in 90 h) and the molecular weight distribution is controlled. These results demonstrate that ROP of ZLys-NCA improves the control of molecular weight distribution and elimination of side reactions by replacing primary amine with amine hydrochloride. These diblock copolymers characterized by GPC (Figure 7b) and ^{1}H NMR and results are summarized in Table 2 (expt 1 and expt 2). Then in a second reaction step, the Cbz protective side chains were removed by treating these block copolymers with HBr/AcOH in trifluoroacetic acid and the resulting block copolymer was characterized by ^{1}H NMR. The spectra before and after deprotection of the Cbz groups for expt 1 are shown in Figure 8. Comparing the peak integral ratio (Figure 8a) of the methine protons of PNIPAm (C*H* δ 3.8) and the methylene protons of the Z group ($CH_2C_6H_5$ δ 4.9), the DP of PZLys is 71. After deprotecting of the PNIPAm-*b*-PZLys, the peak integral ratio (Figure 8b) of the methine protons of PNIPAm (C*H* δ3.8) and α-methine protons of PLys (COC*H*NH δ 4.2) result in DP of 72. On the basis of the ^{1}H NMR calculation, we confirmed that there was neither loss of the lysine repeating units by backbone scission nor cleavage of the amide group to a secondary amino group in the PNIPAm block. Therefore, we can ascertain that the polymerization of Z-Lys-NCA and deprotection of Cbz groups are successfully accomplished by using the amine hydrochloride-functionalized PNIPAm. The polydispersity of PNIPAm$_{90}$-*b*-PZLys$_{71}$ is about 1.20, and the DP is close to the value predicted from the initial monomer/macroinitiator ratio. In a similar fashion, ROP of BLG-NCA was also performed by PNIPAm-$NH_3^+Cl^-$ and results are summarized in Table 2 (expt 3 and 4). However, the kinetic study gives noticeable broader molecular weight distribution (see Supporting Information for GPC traces, Figure S3). According to recent work demonstrated by Meyer and Schlaad,[37] the rate of polymerization is mainly determined by the position of the ammonium−amine equilibrium, thus the more polar solvent, the softer counterion, and the higher temperature will accelerate the polymerization rate. Since the polymerization of NCA conditions in this study were the same, we attribute the faster polymerization rate of BLG-NCA to more polar BLG-NCA monomer and result in less control of the growing polymer chain end during the course of the polymerization. These diblock copolymers were charac-

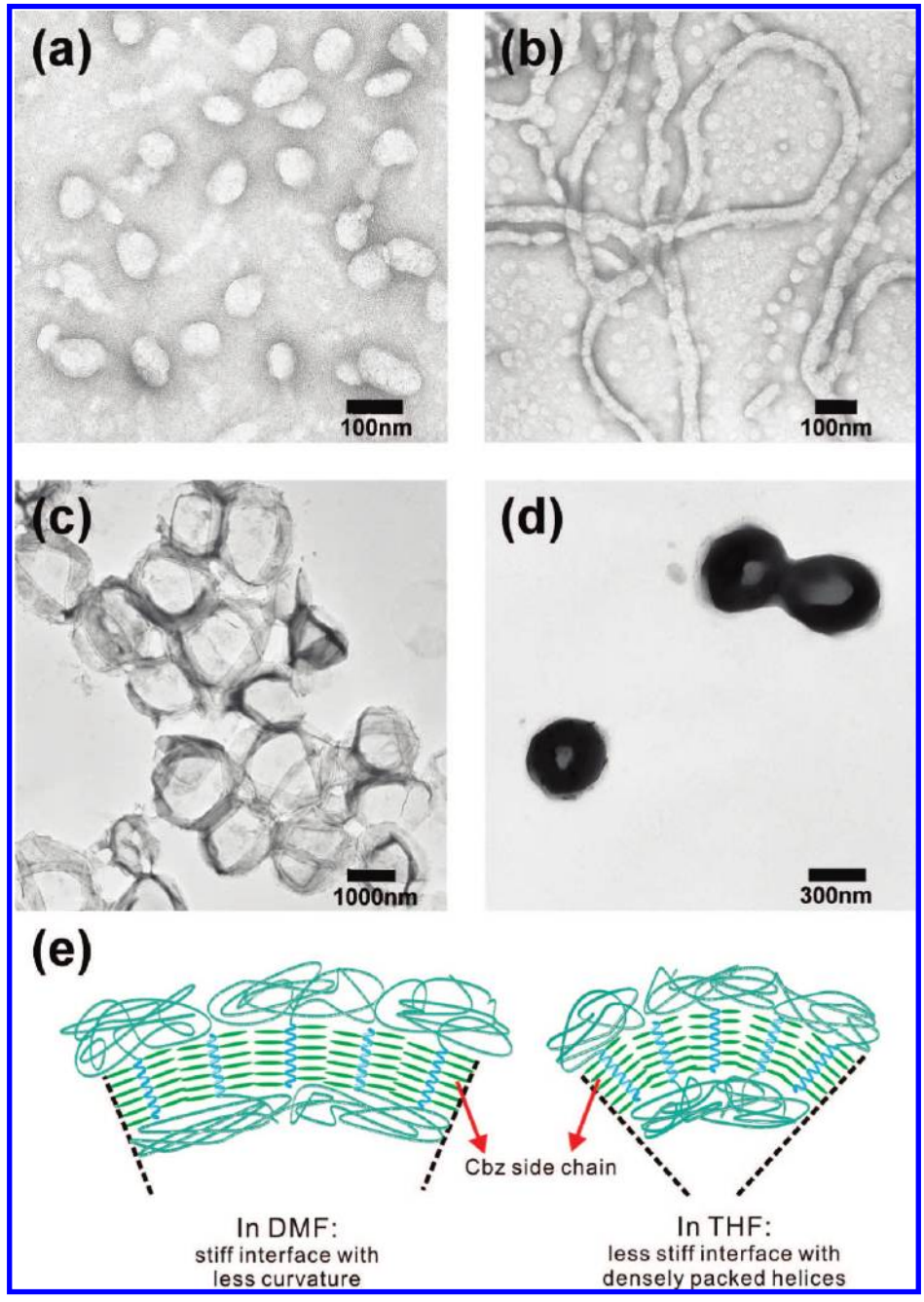

Figure 9. TEM images of PNIPAm$_{197}$-*b*-PZLys$_{44}$ (a, b) and PNIPAm$_{90}$-*b*-PZLys$_{71}$ (c, d): (a) spherical micelles morphology, (b) mixed spherical and wormlike micelles morphology, (c) giant vesicles morphology, and (d) compact vesicles morphology. (e) Schematic representation of the proposed self-assembly behaviors of PNIPAm$_{90}$-*b*-PZLys$_{71}$ into vesicles morphology by using different common helicogenic solvents.

terized by GPC (Figure S4) and ^{1}H NMR and results are summarized in Table 2 (expt 3 and 4).

Self-Assembly Behavior of PNIPAm-*b*-PZLys Diblock Copolymer in Aqueous Solution. Most prior studies on self-assembly of polypeptides in dilute solution have concentrated on the determination of the influences of various parameters such as molecular weight, solvent, temperature, salt, pH, amino acid composition, etc.[38] However, little attention has been paid to the self-assembly properties based on Cbz-protective side chain polypeptide amphiphilic block copolymers in aqueous medium.[39] It is well-known that polypeptide forms α-helical conformation, a tight spiral stabilized by hydrogen bonds. This ensures that the PNIPAm-*b*-PZLys copolymer has rodlike hydrophobic and flexible hydrophilic segment. In order to investigate the rod−coil self-assembly in aqueous solution, we selected two samples of diblock copolymers, PNIPAm$_{197}$-*b*-PZLys$_{44}$ and PNIPAm$_{90}$-*b*-PZLys$_{71}$, to observe aggregation morphology by transmission electron microscopy (TEM). These two samples were first dissolved in helicogenic common solvent (DMF or THF) and then precipitant (water) was added to the solution. After stirring for 2 days for equilibrium, organic solvent was removed from the colloidal solution by dialyzing against DI water and observed by TEM. Depending on the nature of organic solvent employed, the morphology of aggregates formed in DMF/water system may differ to that in THF/water. In addition, the copolymer composition is another effective approach to affect the aggregate morphology. In the system of PNIPAm$_{197}$-*b*-PZLys$_{44}$, the micelle morphologies changed from a spherical micelle in DMF/water system to a mixed spherical and wormlike micelle in THF/water system as shown in Figure 9, a and b. Nakajima et al. reported that the Cbz side chain dimension varies in accordance with the kind of solvent dipole

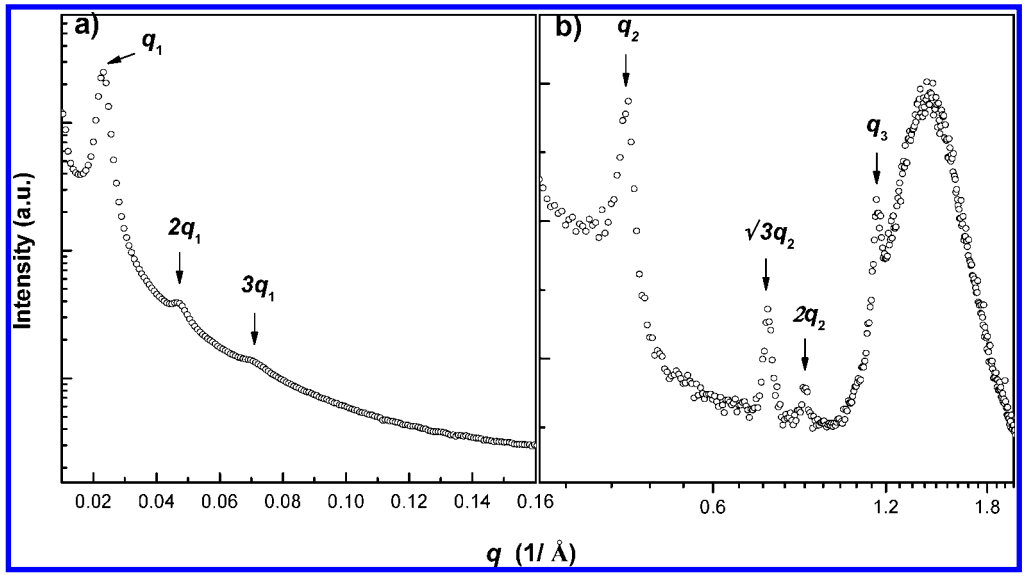

Figure 10. (a) SAXS and (b) WAXS patterns of the PNIPAm$_{90}$-*b*-PZLys$_{71}$ recorded at room temperature.

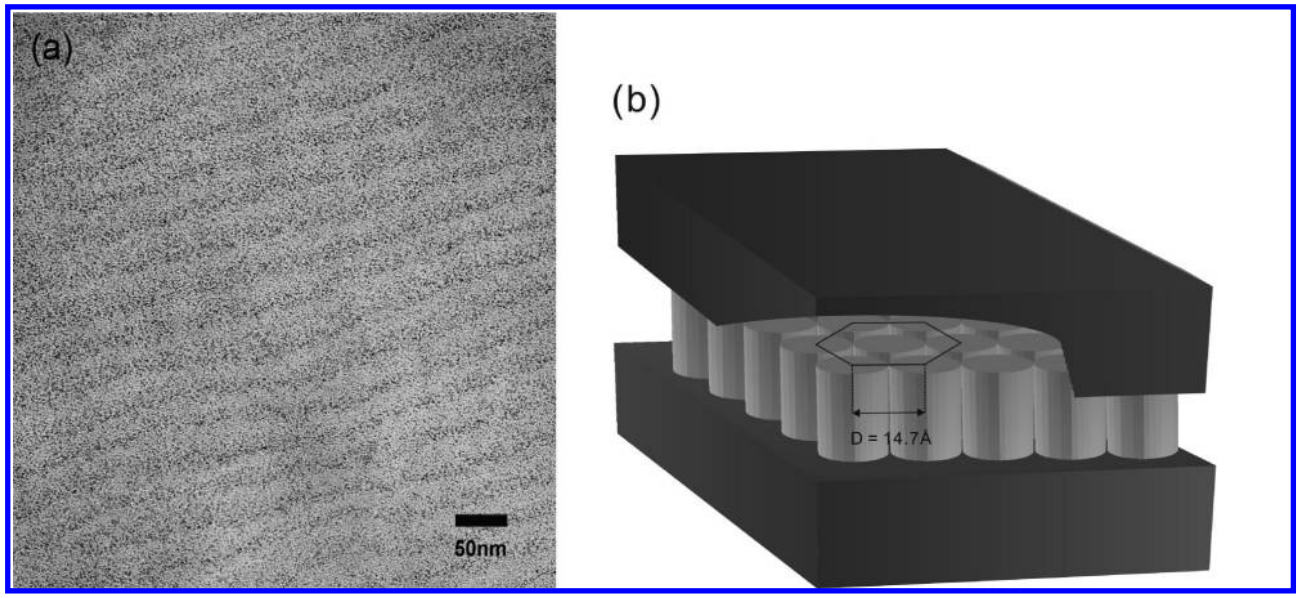

Figure 11. (a) TEM image of the PNIPAm$_{90}$-*b*-PZLys$_{71}$ lamellar phase separation morphology. Note that polypeptide regions appear black due to staining with RuO_4. (b) Proposed schematic representation of the hexagonal-in-lamellar solid-state morphology of PNIPAm-*b*-PZLys block copolymer.

moment.[40] The solvent with high dipole moment possesses greater dimension for the side chain originating from the difference in the side chain−solvent interaction. Consequently, when the common solvent is changed from DMF to THF, a less dipole moment solvent of THF, it tends to induce rod segment side chain to shrink. The rodlike peptide helices can pack side-by-side along their long axes to form more compact micelle core in THF/water than that in DMF/water system. However, there was not enough space to accommodate the relatively longer solvent-compatible PNIPAm block in the corona domain. Consequently, in order to reduce the repulsion contribution of corona-forming PNIPAm block, the morphology shifts to mixed spherical and wormlike micelles for decreasing the corona free energy.[41] Furthermore, all of the spherical micelles observed in THF/water system are smaller than those in the DMF/water system, suggesting that the core-forming PZLys chains are packed more densely. The effect of copolymer composition on morphological change was investigated by examining other sample of PNIPAm$_{91}$-*b*-PZLys$_{71}$. When the PZLys composition f_{PZLys} is increased from 0.18 to 0.44, the morphology changes from spherical micelles to giant vesicles in the DMF/water system (Figure 9c), and from mixed spherical and wormlike micelles to vesicles in THF/water system (Figure 9d). Decreasing f_{PNIPAm} reduces the corona crowding and thus permits a larger aggregation number. However, expansion of the sphere is inhibited by the large entropy penalty from increasing f_{PZLys}.[42] Consequently, the micelle morphology changes to giant vesicles to satisfy the less interfacial curvature requirement for the relatively shorter PNIPAm and the stiff interface from packed helices. The common solvent THF also leads to vesicle aggregates but in smaller dimension about 430 nm. According to the above discussion, in the THF/water system compact vesicles can be attributed to the less stiff interface of the more densely packed helices and its corresponding segments length. Figure 9e depicts the proposed self-assembly behaviors of the diblock copolymer PNIPAm$_{91}$-*b*-PZLys$_{71}$ into vesicles by using different common helicogenic solvents with varied Cbz side chain dimension. In this section, the micelle morphologies of PNIPAm-*b*-PZLys in both DMF/water and THF/water system are characterized. These am-

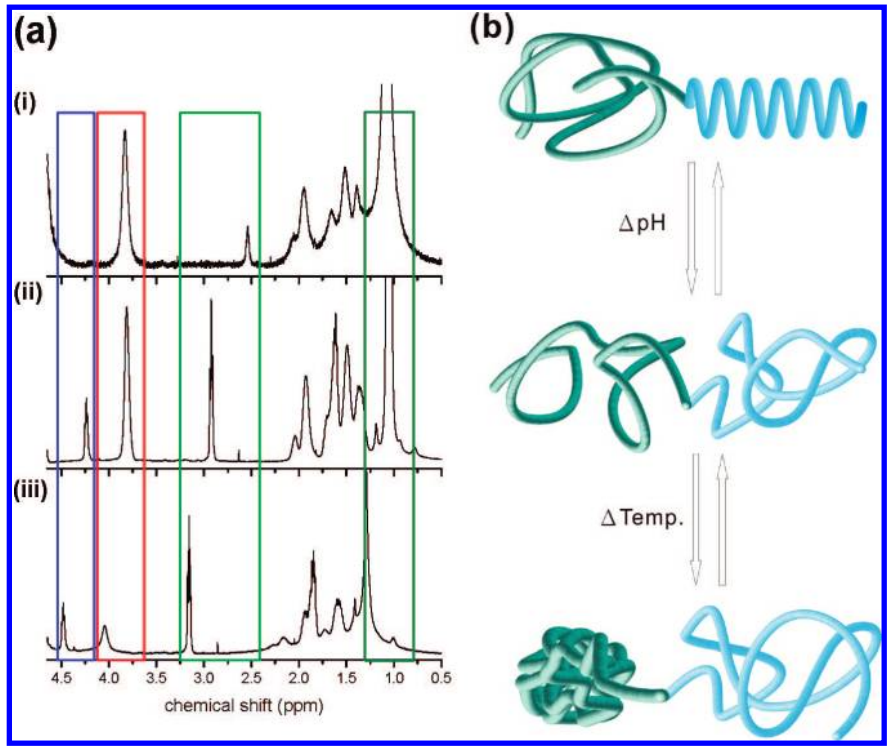

Figure 12. (a) ^{1}H NMR spectra recorded in D_2O: (i) PNIPAm$_{197}$-*b*-PLys$_{44}$ at pH = 13, (ii) PNIPAm$_{197}$-*b*-PLys$_{44}$ at pH = 7, and (iii) PNIPAm$_{197}$-*b*-PLys$_{44}$ at 45 °C. (b) Proposed schematic representation of the PNIPAm$_{197}$-*b*-PLys$_{44}$ stimuli-responsive behavior of the pH-induced coil-to-helix and thermo-induced coil-to-globule transition in aqueous solution.

phiphilic hybrid rod−coil block copolymers are able to form well-defined universal morphologies upon varying copolymer compositions and the helicogenic common solvents.

Hierarchical Self-Assembly Structure of PNIPAm-*b*-PZLys Rod−Coil Block Copolymer in Solid State. Almost 30 years ago, Gallot et al.[43] investigated the solid-state behavior of polyvinyl-*b*-polypeptide rod−coil diblock copolymers by small-angle X-ray scattering (SAXS). They found a large-scale hexagonal-in-lamellar morphology of the alternating polyvinyl and polypeptide sheets with the α-helical polypeptide chains arranged in a hexagonal array. In order to investigate this new polypeptide-based rod−coil copolymer, synchrotron SAXS, wide-angle X-ray scattering (WAXS), and TEM techniques were used to examine solid-state nanodomain morphology and the polypeptide secondary structure. SAXS and WAXS spectra for the PNIPAm$_{90}$-*b*-PZLys$_{71}$ are shown in Figure 10. For SAXS pattern in Figure 10a, orders of sharp reflection with relative positions 1:2:3 indicate a very high quality of lamellar microphase separation structure with nanodomain distance of 27.3 nm. The WAXS pattern can be used to identify the secondary polypeptide structure. The WAXS curve in Figure 10b exhibits PZLys peaks with relative positions 1:$\sqrt{3}$:$\sqrt{4}$ corresponding to hexagonally packed α-helices secondary structures. The set of diffraction peaks at the largest reflection (~0.43 Å^{-1}) corresponds to a *d* spacing of ~14.7 Å which can be attributed to the intercolumnar distance of PZLys chains into a columnar hexagonal lattice. The reflection at 11.5 Å^{-1} corresponds to the pitch of the helix of 5.4 Å. The broad "amorphous halo" centered around 14.1 Å^{-1} (with a corresponding average distance of 4.5 Å) carries a large fraction of the diffracted intensity originating form the long amorphous side chains. In order to gain more information about the structural details, the morphology was also analyzed by TEM to gain the conformation of a single block copolymer chain. In Figure 11a, the lamellar morphology was observed and the maximum length of the α-helices (1.5 Å × 71 = 106.5 Å) is comparable to the thickness of poly(Z-L-lysine) layer in TEM graph. This would indicate that the helices are not stacked but are rather interdigitated or rarely folded.[44] This could be attributed to the polypeptide α-helices producing a strong electric dipole moment along the molecule axis; both interdigitation and helix folding are ways to minimize the energy of the superstructure of helices. The schematic representation of the expected structure is shown in Figure 11b. On the basis of these results, the self-assembly structure is a lamellar-in-hexagonal (LH) morphology, referring to the local hexagonal packing of the α-helical polypeptide chains and the phase segregation into a lamellar structure.

Stimuli-Responsive Behavior of PNIPAm-*b*-PLys Diblock Copolymer in Aqueous Solution. ^{1}H NMR spectroscopy was used to investigate the dual stimuli-responsive behavior of PNIPAm$_{197}$-*b*-PLys$_{44}$. Upon dissolution of the diblock copolymer in basic or thermal D_2O solution (the D_2O solution temperature was raised above the LCST of PNIPAm block from 25 °C to a thermal state at 45 °C), the conformation changed spontaneously as demonstrated by ^{1}H NMR. Spectra of the diblock copolymer were obtained in basic (pH ≈ 13, NaOD/D_2O) or thermal condition at 45 °C and compared with that in neutral D_2O at 25 °C (Figure 12a). Under basic condition, the protonated ($-NH_3^+$) poly(L-lysine) block is transformed into neutral and insoluble $-CH_2-NH_2$ groups supported by observation of several chemical shifts. The signal at 2.92 ppm ($-CH_2-NH_3^+$) appeared in neutral D_2O becomes a weak intensity at 2.54 ppm, and the α-methine protons of PLys (COC*H*NH) at 4.2 ppm almost completely disappears, indicating that its secondary conformation changes from a charged coil to a neutral and compact α-helical structure, while the PNIPAm segment remains fully solvated. These phenomena are in line with the results previously reported for coil-helix transition of poly(L-lysine).[45] Similarly, when the temperature is elevated up to 45 °C, the signal at 3.81 and 1.06 ppm, corresponding to the PNIPAm methine and methyl

protons peak intensity, become attenuated relative to the PLys methylene peak. Although the mechanism for the LCST behavior is complex, it is generally accepted that the LCST behavior or phase transition of NIPAM-based polymers is associated with the dehydration of the chains, which leads to a more compact structure.[46] Figure 12b depicts the proposed model of the dual stimuli-responsive structure.

Conclusions

We have demonstrated that an amide-linkage heterofunctional initiator was successfully synthesized which allows polymerization to be conducted consecutively by atom transfer radical polymerization and then the amine hydrochloride mediated ring-opening polymerization of α-amino acid *N*-carboxyanhydrides. Well-defined poly(*N*-isopropylacrylamide)-*b*-poly(Z-L-lysine) was obtained and the protective Cbz-group was successfully removed without cleavage of the block copolymer. We found that the amphiphilic hybrid rod−coil block copolymers were able to form various well-defined universal morphologies including micelles−spherical micelles, wormlike micelles, and vesicles by varying either the copolymer compositions or the helicogenic common solvents. On the basis of synchrotron SAXS, WAXS, and TEM results, we have confirmed the formation of the hierarchical lamellar-in-hexagonal self-assembly structure in $PNIPAm_{90}$-*b*-$PZLys_{71}$ at solid state. By removing the protective Cbz-group, the dual stimuli-responsive behaviors of the PNIPAm-*b*-PLys were investigated by nuclear magnetic resonance spectroscopy in aqueous solution. Coil-to-helix and coil−globule transitions occur by changing the environmental conditions, by elevating the temperature or changing the pH value.

This work has demonstrated the feasibility of using heterofunctional amide linkage initiator to synthesize hybrid block copolymers which both segments are able to response to environmental changes. In the effort to expand potential applications, these results presented here provide a versatile method toward designing polymers to impart stimuli-responsive functionalities.

Acknowledgment. This study was supported financially by the Ministry of Education's "Aim for the Top University" (MOEATU) program and the National Science Council, Taiwan (contract no. NSC-95-2221-E-009-118).

Supporting Information Available: GPC traces of the functionalized macroinitiators dialyzed in two temperature water bath and the PNIPAm-*b*-polypeptides. This material is available free of charge via the Internet at http://pubs.acs.org.

References and Notes

(1) Hamley, I. W. *Angew. Chem., Int. Ed.* **2003**, *42*, 1692–1712.
(2) Ambade, A. V.; Savariar, E. N.; Thayumanavan, S. *Mol. Pharm.* **2005**, *2*, 264–272.
(3) Elbert, D. L.; Herbert, C. B.; Hubbell, J. A. *Langmuir* **1999**, *15*, 5355–5362.
(4) Cai, Q.; Zeng, K.; Ruan, C.; Decai, T. A.; Grimes, C. A. *Anal. Chem.* **2004**, *76*, 4038–4043.
(5) Schild, H. G. *Prog. Polym. Sci.* **1992**, *17*, 163–249.
(6) Poe, G. D.; Jarrett, W. L.; Scales, C. W.; McCormick, C. L. *Macromolecules* **2004**, *37*, 2603.
(7) Virtanen, J.; Arotcarena, M.; Heise, B.; Ishaya, S.; Laschewsky, A.; Tenhu, H. *Langmuir* **2002**, *18*, 5360–5363.
(8) (a) Bellomo, E.; Wyrsta, M. D.; Pakstis, L.; Pochan, D. J.; Deming, T. J. *Nat. Mater.* **2004**, *3*, 244–248. (b) Holowka, E. P.; Pochan, D. J.; Deming, T. J. *J. Am. Chem. Soc.* **2005**, *127*, 12423–12428. (c) Rodríguez-Hernández, J.; Lecommandoux, S. *J. Am. Chem. Soc.* **2005**, *127*, 2026–2027. (d) Nowak, A. P.; Breedveld, V.; Pakstis, L.; Ozbas, Bl.; Pine, D. J.; Pochan, D.; Deming, T. J. *Nature (London)* **2002**, *417*, 424–428.
(9) Mart, R. J.; Osborne, R. D.; Stevens, M. M.; Ulijn, S. V. *Soft Matter* **2006**, *2*, 822–835.
(10) Schlaad, H.; Antonietti, M. *Eur. Phys. J. E* **2003**, *10*, 17–23.
(11) (a) Babin, J.; Rodríguez.Hernández, J.; Lecommandoux, S.; Klok, H.-A.; Achard, M.-F. *Faraday Discuss.* **2005**, *128*, 179–192. (b) Chécot, F.; Lecommandoux, S.; Gnanou, Y.; Klok, H.-A. *Angew. Chem., Int. Ed.* **2002**, *41*, 5752–5784. (c) Börner, H. G.; Schlaad, H. *Soft Matter* **2007**, *3*, 394–408. (d) Gebhardt, K. E.; Ahn, S.; Venkatachalam, G.; Savin, D. A. *Langmuir* **2007**, *23*, 2851–2856.
(12) Kricheldorf, H. R. *Angew. Chem., Int. Ed.* **2006**, *45*, 5752–5784.
(13) Deming, T. J. *J. Polym. Sci., Part A: Polym. Chem.* **2000**, *38*, 3011–3018.
(14) (a) Deming, T. J. *Nature (London)* **1997**, *390*, 386–389. (b) Deming, T. J. *Adv. Drug Deliv. Rev.* **2002**, *54*, 1145–1155.
(15) Brzezinska, K. R.; Deming, T. J. *Macromolecules* **2001**, *34*, 4348–4354.
(16) Aliferis, T.; Iatrou, H.; Hadjichristidis, N. *Biomacromolecules* **2004**, *5*, 1653–1656.
(17) Dimitrov, I.; Schlaad, H. *Chem. Commun.* **2003**, *23*, 2944–2945.
(18) (a) Dimitrov, I.; Kukula, H.; Cölfen, H.; Schlaad, H. *Macromol. Symp.* **2004**, *215*, 383–393. (b) Lutz, J.-F.; Schutt, D.; Kubowicz, S. *Macromol. Rapid Commun.* **2005**, *26*, 23–28. (c) Meyer, M.; Schlaad, H. *Macromolecules* **2006**, *39*, 3967–3970. (d) Dimitrov, I.; Berlinova, I. V.; Vladimirov, N. G. *Macromolecules* **2006**, *39*, 2423–2426.
(19) (a) Matyjaszewski, K. *Prog. Polym. Sci.* **2005**, *30*, 858–875. (b) Braunecker, W. A.; Matyjaszewski, K. *Prog. Polym. Sci.* **2007**, *32*, 93–146. (c) Matyjaszewski, K.; Xia, J. *Chem. Rev.* **2001**, *101*, 2921–2990. (d) Kamigaito, M.; Ando, T.; Sawamoto, M. *Chem. Rev.* **2001**, *101*, 3689–3746.
(20) Bernaerts, K. V.; Du Prez, F. E. *Prog. Polym. Sci.* **2005**, *30*, 858–875.
(21) Rao, J.; Luo, Z.; Ge, Z.; Liu, H.; Liu, S. *Biomacromolecules* **2007**, *8*, 3871–3878.
(22) Schild, H. G. *Prog. Polym. Sci.* **1992**, *17*, 163–249.
(23) Xia, Y.; Yin, X.; Burke, N. A. D.; Stover, H. D. H. *Macromolecules* **2005**, *38*, 5937–5943.
(24) Hawker, C. J.; Bosman, A. W.; Harth, E. *Chem. Rev.* **2001**, *101*, 3661–3688.
(25) (a) Ray, B.; Isobe, Y.; Matsumoto, K.; Habaue, S.; Okamoto, Y.; Kamigaito, M.; Sawamoto, M. *Macromolecules* **2004**, *37*, 1702–1710. (b) Convertine, A. J.; Ayres, N.; Scales, C. W.; Lowe, A. B.; McCormick, C. L. *Biomacromolecules* **2004**, *5*, 1177–1180.
(26) Poché, D.; Moore, M.; Bowles, J. *Synth. Commun.* **1999**, *29*, 843–854.
(27) Ciampolini, M.; Nardi, N. *Inorg. Chem.* **1966**, *5*, 41–44.
(28) Baek, K.-Y.; Kamigaito, M.; Sawamoto, M. *J. Polym. Sci., Part A: Polym. Chem.* **2002**, *40*, 1937–1944.
(29) (a) Xu, F. J.; Zhong, S. P.; Yung, L. Y. L.; Kang, E. T.; Neoh, K. G. *Biomacromolecules* **2004**, *5*, 2392–2403. (b) Limer, A.; Haddleton, D. M. *Macromolecules* **2006**, *39*, 1353–1358. (c) Venkataraman, S.; Wooley, K. L. *Macromolecules* **2006**, *39*, 9661–9664.
(30) (a) Neugebauer, D.; Mtyjaszewski, K. *Macromolecules* **2003**, *36*, 2598–2603. (b) Masci, G.; Giacomelli, L.; Crescenzi, V. *Macromol. Rapid Commun.* **2004**, *25*, 559–564. (c) Teodorescu, M.; Mtyjaszewski, K. *Macromol. Rapid Commun.* **2000**, *21*, 190–194.
(31) Matyjaszewski, K.; Shipp, D. A.; Wang, J.-L.; Grimaud, T.; Patten, T. E. *Macromolecules* **1998**, *31*, 6836–6840.
(32) Fischer, H. *Chem. Rev.* **2001**, *101*, 3581–3610.
(33) (a) Tang, W.; Matyjaszewski, K. *Macromolecules* **2006**, *39*, 4953–4959. (b) Tang, W.; Matyjaszewski, K. *Macromolecules* **2007**, *40*, 1858–1863.
(34) Matyjaszewski, K.; Nakagawa, Y.; Gaynor, S. G. *Macromol. Rapid Commun.* **1997**, *18*, 1057.
(35) Harrisson, S.; Wooley, K. L. *Polym. Prep.* **2004**, *45*, 545–546.
(36) Postma, A.; Davis, T. P.; Moad, G.; O'Shea, M. S. *React. Funct. Polym.* **2006**, *66*, 137–147.
(37) Schlaad, H.; Meyer, M. *PMSE Prepr.* **2007**, *97*, 183–184.
(38) Schlaad, H. *Adv. Polym. Sci.* **2006**, *202*, 53–73.
(39) (a) Naka, K.; Yamashita, R.; Nakamura, T.; Ohki, A.; Maeda, S. *Macromol. Chem. Phys.* **1997**, *198*, 89–100. (b) Cheon, J. B.; Jeong, Y. I.; Cho, C. S. *Polymer* **1999**, *40*, 2041–2050. (c) Toyotama, A.; Kugimiya, S. I.; Yamanaka, J.; Yonese, M. *Chem. Pharm. Bull.* **2001**, *49*, 169–172. (d) Tang, D.; Lin, J.; Lin, S.; Zhang, S.; Chen, T.; Tian, X. *Macromol. Rapid Commun.* **2004**, *25*, 1241–1246. (e) Dong, C. M.; Sun, X. L.; Fauche, K. M.; Apkarian, R. P.; Chaikof, E. L. *Biomacromolecules* **2004**, *5*, 224–231.
(40) Ishimuro, Y.; Hamada, F.; Nakajima, A. *Macromolecules* **1978**, *11*, 382–387.
(41) (a) He, Y.; Li, Z.; Simone, P.; Lodge, T. P. *J. Am. Chem. Soc.* **2006**, *128*, 2745–2750. (b) Bhargava, P.; Zheng, J. X.; Li, P.; Quirk, R. P.; Harris, F. W.; Cheng, S. Z. D. *Macromolecules* **2006**, *39*, 4880−4888.
(42) Zhang, L.; Eisenberg, A. *Polym. Adv. Technol.* **1998**, *9*, 677–699.

(43) (a) Billot, J. P.; Douy, A.; Gallot, B. *Makromol. Chem.* **1976**, *177*, 1889–1893. (b) Billot, J. P.; Douy, A.; Gallot, B. *Makromol. Chem.* **1977**, *178*, 1641–1650. (c) Gallot, B. *Prog. Polym. Sci.* **1996**, *21*, 1035–1088.

(44) (a) Douy, A.; Gallot, B. *Polymer* **1982**, *23*, 1039–1044. (b) Losik, M.; Kubowicz, S.; Smarsly, B.; Schlaad, H. *Eur. Phys. J. E* **2004**, *15*, 407–411. (c) Schlaad, H.; Kukula, H.; Smarsly, B.; Antonietti, M.; Pakula, T. *Polymer* **2002**, *43*, 5321–5328. (d) Schlaad, H.; Smarsly, B.; Losik, M. *Macromolecules* **2004**, *37*, 2210–2214. (e) Lecommandoux, S.; Achard, M. F.; Langenwalter, J. F.; Klok, H. A. *Macromolecules* **2001**, *34*, 9100–9111.

(45) Bradbury, E. M.; Crane-Robinson, C.; Goldman, H.; Rattle, H. W. E. *Biopolymers* **1968**, *6*, 851–862.

(46) Ono, Y.; Shikata, T. *J. Am. Chem. Soc.* **2006**, *128*, 10030–10031.

MA801221M